Multiband Orange-Red Luminescence of Eu^{3+} Ions Based on the Pyrochlore-Structured Host Crystal

Shinobu Fujihara* and Kazuaki Tokumo

Department of Applied Chemistry, Faculty of Science and Technology, Keio University, 3-14-1 Hiyoshi, Kohoku-ku, Yokohama 223-8522, Japan

Received June 25, 2005. Revised Manuscript Received September 2, 2005

Pyrochlore-type yttrium stannate ($Y_2Sn_2O_7$) doped with trivalent europium ions (Eu^{3+}) was synthesized as thin films by the sol−gel method. X-ray diffractometry, high-resolution transmission electron microscopy, and X-ray photoelectron spectroscopy were used to evaluate the crystallinity and purity of the films, which was of prime importance in investigating the optical properties. It was shown that heat treatment of the films at 1000 °C was enough to obtain highly crystalline and phase-pure samples. Photoluminescence spectra of the $(Y_{1-x}Eu_x)_2Sn_2O_7$ ($x = 0.01-0.20$) films indicated the simultaneous occurrence of five predominant orange-red band emissions at a single-wavelength ultraviolet excitation due to doubly split magnetic−dipole $^5D_0 \rightarrow {}^7F_1$ and electric−dipole $^5D_0 \rightarrow {}^7F_2$ transitions. Inhomogeneous broadening possibly arising from the site-to-site variation of Eu^{3+} was also observed. These results demonstrate that we have succeeded in synthesizing a single-phase crystalline phosphor material having the chromaticity corresponding to a region between pink and yellowish pink.

1. Introduction

Red luminescence of trivalent europium (Eu^{3+}) ions due to intraconfigurational f−f transitions is of technological importance because it has been widely applied to phosphors for color displays and fluorescent lamps.[1−3] It is known that emission wavelengths of Eu^{3+} are determined primarily by their local environment in host crystals. That is, the probability of electronic transitions from the lowest $^5D_0$ excited state to the $^7F_{0-6}$ ground states differs depending on site symmetries. At a site without inversion symmetry, Eu^{3+} exhibits the hypersensitive forced electric−dipole $^5D_0 \rightarrow {}^7F_2$ transition with emission wavelengths of approximately 610−620 nm. In contrast, the allowed magnetic−dipole $^5D_0 \rightarrow {}^7F_1$ transition is usually observed at around 592 nm from Eu^{3+} located at a site with inversion symmetry. Actually, both the electric−dipole and the magnetic−dipole transitions appear simultaneously in practical inorganic luminescent materials, although their intensities are different and, in most cases, one of which is much stronger. Therefore, the asymmetry ratio,[4] which is defined as the intensity ratio between the $^5D_0 \rightarrow {}^7F_2$ and $^5D_0 \rightarrow {}^7F_1$ transitions, is always far from unity. Furthermore, the $^7F_{0-6}$ ground states undergo crystal-field splitting, which also influences the emission wavelengths of all $^5D_0 \rightarrow {}^7F_{0-6}$ transitions.[1]

A certain application of Eu^{3+}-activated phosphors prefers multiband emissions rather than a monochromatic sharp emission. For example, emissions of Eu^{3+} can produce reddish components of artificial white light. When spectral features of white light need to be similar to those of the natural light (sunlight), the multiband Eu^{3+} emissions are expected to be quite useful because of the better spectral overlap. Development of novel phosphors is, therefore, one of the most important aspects in designing luminescent devices. Eu^{3+} occupies several symmetry sites in oxide glasses, resulting in inhomogeneous broadening in emission spectra.[5] However, the $^5D_0 \rightarrow {}^7F_2$ transition is relatively stronger than the $^5D_0 \rightarrow {}^7F_1$ one due to the lower symmetry of the Eu^{3+} sites. Furthermore, absorption or excitation spectra also undergo inhomogeneous broadening, which is in turn undesirable for efficient charge-transfer or host interband excitations to occur. Consequently, it is more promising to use crystalline hosts providing lattice sites with little dispersion of symmetries. To realize multiband emissions, site symmetries should be lowered to a certain extent by chemical modification of hosts through making solid solutions or introducing lattice defects.

Pyrochlore oxides, expressed by the general formula of $A_2B_2O_7$, have a structure derived from the fluorite. Two kinds of cations are ordered on the *A* and *B* sites, and one-eighth of the anions are missing with ordered vacancies. Disordering of the cation sites coupled with oxygen disorder on the anion vacancies within the pyrochlore structure results in a defect-fluorite structure.[6] One of the most promising applications of pyrochlore oxides is as anionic conductors due to their high-temperature stability.[7] When one considers application of pyrochlore oxides as Eu^{3+}-activated luminescent materials,

* To whom correspondence should be addressed. Phone: +81 (0)45-566-1581. Fax: +81 (0)45-566-1551. E-mail: shinobu@applc.keio.ac.jp.

(1) Blasse, G.; Grabmaier, B. C. *Luminescent Materials*; Springer-Verlag: Berlin, 1994.
(2) Yacobi, B. G.; Holt, B. G. *Cathodoluminescence Microscopy of Inorganic Solids*; Plenum Press: New York, 1990.
(3) Chakhovskoi, A. G.; Kesling, W. D.; Trujillo, J. T.; Hunt, C. E. *J. Vac. Sci. Technol., B* **1994**, *12*, 785.
(4) Ollier, N.; Concas, G.; Panczer, G.; Champagnon, B.; Charpentier, T. *J. Non-Cryst. Solids* **2003**, *328*, 207.
(5) Reisfeld, R.; Ziganski, E.; Gaft, M. *Mol. Phys.* **2004**, *102*, 1319.
(6) Panero, W. R.; Stixrude, L.; Ewing, R. C. *Phys. Rev. B* **2004**, *70*, 054110.
(7) Boivin, J. C.; Mairesse, G. *Chem. Mater.* **1998**, *10*, 2870.

10.1021/cm0513785 CCC: $30.25
Published on Web 10/08/2005

yttrium-containing pyrochlores (A = Y and B = Sn, Ti, Zr) seem to be suitable because of their potential capability of accommodating Eu^{3+} in the Y^{3+} site, as observed in the common Y_2O_3:Eu^{3+} red phosphor.[8]

In this article we report the luminescence behavior of Eu^{3+} ions introduced in a $Y_2Sn_2O_7$ host crystal that has a high Y^{3+} site symmetry. Thin-film specimens of $(Y_{1-x}Eu_x)_2Sn_2O_7$ were prepared by the sol−gel method to assess correctly optical properties such as absorption and photoluminescence. It was found that $(Y_{1-x}Eu_x)_2Sn_2O_7$ could exhibit multiband orange-red photoluminescence with five intense emission peaks centered at 577, 588, 596, 610, and 628 nm. The chromaticity then corresponded to a region between pink and yellowish pink in the Commission Internationale d′Eclairage (CIE) diagram.

2. Experimental Methods

Reagent-grade yttrium acetate tetrahydrate ($Y(CH_3COO)_3{\cdot}4H_2O$), europium acetate tetrahydrate ($Eu(CH_3COO)_3{\cdot}4H_2O$), and tin(IV) chloride pentahydrate ($SnCl_4{\cdot}5H_2O$) were obtained from Wako Pure Chemicals, Japan. $Y(CH_3COO)_3{\cdot}4H_2O$ (2.5 mmol) and $SnCl_4{\cdot}5H_2O$ (2.5 mmol) were added to ethanol (17 mL) containing nitric acid (3 mL) to prepare precursor solutions. In fabricating Eu^{3+}-doped $Y_2Sn_2O_7$ films, $Eu(CH_3COO)_3{\cdot}4H_2O$ was further added to the solutions. The concentrations of Eu^{3+} as a dopant were varied between 1.0, 5.0, 8.0, 10.0, 12.0, 14.0, and 20.0 at. % against Y^{3+}, expecting final film compositions of $(Y_{1-x}Eu_x)_2Sn_2O_7$ (x = 0.01−0.20). Citric acid (10 mmol, Wako), working as a chelating agent, and poly(ethylene glycol) (PEG) (40 mmol in terms of monomer, Wako, molecular weight of 20000), working as a cross-linking agent, were mixed with the solutions by stirring for 24 h at room temperature. The resultant solutions were then dip-coated on quartz glass substrates, immediately placed in a furnace preheated to a temperature between 500 and 1000 °C, and heated there for 1 h in air followed by quenching. Although the quartz glass substrates were thought to be inert in terms of the reactivity with the films deposited, we paid particular attention to the possible formation of silicate-related byproducts because they might influence the luminescent behavior of Eu^{3+}. X-ray photoelectron spectroscopy (XPS) was therefore used to analyze the film composition.

Thermal analysis of the solution that was dried at 100 °C for 1 week was carried out using thermogravimetry−differential thermal analysis (TG−DTA) (Mac Science, type TG-DTA2020S). Crystalline phases precipitated in the films were identified using an X-ray diffractometer with a thin-film attachment and Cu Kα radiation (Rigaku). The incident angle was fixed at 0.5°. Angles against the film surface were scanned as 2θ. The film morphology was observed with a field-emission scanning electron microscope (FESEM) (Hitachi, type S-4700). The particle morphology and crystallinity were observed with a high-resolution transmission electron microscope (HRTEM) (Philips, type TECNAI F20). Images were obtained by deposition of the scratched films onto a carbon-covered copper grid. XPS was carried out using Mg Kα radiation for elemental analysis (JEOL, type JSP-9000MC). XPS data was corrected using the C 1s level as a reference. Optical transmission spectra were recorded with a UV−vis spectrophotometer (Hitachi, type U-3300). Photoluminescence spectra were measured at room temperature with a spectrofluorophotometer (Shimadzu, type RF-5300PC) using a xenon lamp (150 W) as a light source. Careful attention was paid to avoid any misinterpretation of the spectra possibly coming from the apparatus and measurement conditions. Emission scans were performed with 1.5 nm band-pass emission slits. A filter, which eliminated light having wavelengths <350 nm, was used to remove a second-order peak of the excitation light.

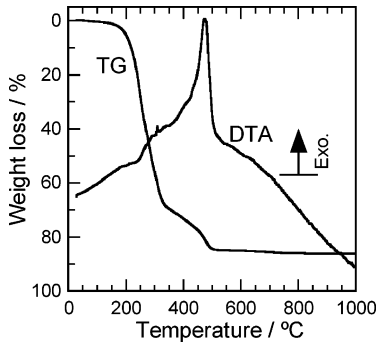

Figure 1. TG−DTA curves of the dried precursor solution.

3. Results and Discussion

3.1. Characterization of Sol−Gel-Derived $Y_2Sn_2O_7$ Films. In the sol−gel processing of crystalline metal oxide materials it is important to examine the thermal decomposition behavior of the precursor solutions containing various kinds of organic compounds. Figure 1 shows TG−DTA curves of the dried solution without europium. The TG curve shows two stages of weight loss. A first large weight loss of approximately 70% is observed at elevated temperatures up to 315 °C, accompanied by a small and broad exothermic DTA peak. This weight loss is due to evaporation of water, ethanol, and citric acid and simultaneously combustion of the organic components, which is usually observed in the sol−gel precursor solutions.[9] A second small weight loss of 15% at temperatures between 315 and 490 °C is followed by a large exothermic peak at 470 °C. This behavior is attributed to combustion of polymers (PEG) that have relatively high thermal durability.[10] The heat-treatment temperature for producing the $Y_2Sn_2O_7$ film should therefore be higher than 500 °C.

Figure 2 shows X-ray diffraction (XRD) patterns of the films obtained by heating the dip-coated precursor solution without europium at temperatures between 500 and 1000 °C for 1 h in air. No appreciable diffraction peaks are seen for the films heated at lower temperatures of 500, 600, and 700 °C, indicating that the films are in an amorphous state. The background appearing in the lower 2θ range in the patterns comes from the quartz glass substrate. Crystallization occurred in the films heated at 800 °C or higher, and their XRD patterns could be indexed with the cubic pyrochlore $Y_2Sn_2O_7$, referring to Joint Committee on Powder Diffraction Standards (JCPDS, file No. 20-1418), having a lattice parameter of 1.0373 nm. The peak intensity increases upon increases in heat-treatment temperature, indicative of the enhanced crystallinity.

A typical FESEM image showing the surface and cross-section morphology is shown in Figure 3 for the $Y_2Sn_2O_7$

(8) Williams, D. K.; Bihari, B.; Tissue, B. M.; McHale, J. M. *J. Phys. Chem. B* **1998**, *102*, 916.
(9) Pang, M. L.; Lin, J.; Cheng, Z. Y.; Fu, J.; Xing, R. B.; Wang, S. B. *Mater. Sci. Eng. B* **2003**, *100*, 124.
(10) Hosono, E.; Fujihara, S.; Onuki, M.; Kimura, T. *J. Am. Ceram. Soc.* **2004**, *87*, 1785.

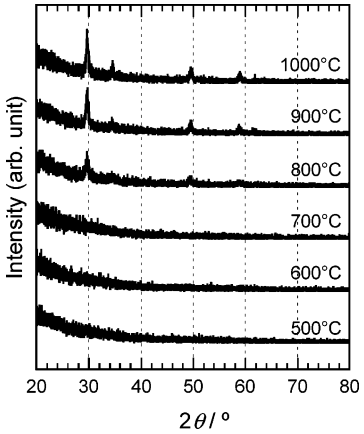

Figure 2. XRD patterns of films obtained by heating the dip-coated precursor solution without europium at temperatures between 500 and 1000 °C for 1 h in air.

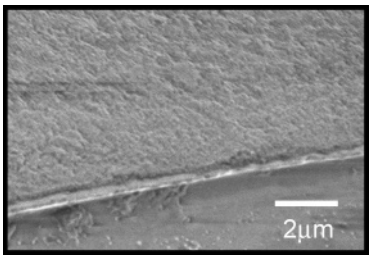

Figure 3. FESEM image of the $Y_2Sn_2O_7$ film heat-treated at 1000 °C.

film heat-treated at 1000 °C. A dense microstructure can be observed with a uniform surface and a film thickness of approximately 150 nm. This morphology is suitable for examination of optical properties because the films are transparent and free from light scattering, as described later. Crystallinity of grains that formed the films was checked by HRTEM. According to the TEM image shown in Figure 4a, the grain size of $Y_2Sn_2O_7$ is observed to be around 30 nm. This size is of the same magnitude as 21 nm derived from the XRD peaks in Figure 2 using the Scherrer equation for the same sample. In addition, the grains are sintered with interparticle necking developed well. The high-magnification HRTEM image shown in Figure 4b clearly presents a lattice image due to phase contrast. The distance between the adjacent lattice fringes corresponds to the interplanar distance of the cubic $Y_2Sn_2O_7$ (222), which is $d_{222} = 0.299$ nm. It can then be said that the $Y_2Sn_2O_7$ film is highly crystalline when heat-treated at a high temperature of 1000 °C.

3.2. Structure of $(Y_{1-x}Eu_x)_2Sn_2O_7$ Films. Figure 5 shows XRD patterns of the $(Y_{1-x}Eu_x)_2Sn_2O_7$ ($x = 0.01-0.20$) films obtained by heating the dip-coated precursor solutions at 1000 °C for 1 h in air. All patterns indicate formation of the pyrochlore-structured phase without any possible other phases such as Y_2O_3, Eu_2O_3, and SnO_2. The intensities and full-width at half-maximum (fwhm) values of the peaks are not influenced by the doping level of x, implying that the crystallinity of the $(Y_{1-x}Eu_x)_2Sn_2O_7$ films is as high as that of the parent $Y_2Sn_2O_7$ film, as mentioned above. As for the pyrochlore, $Eu_2Sn_2O_7$ exists with a cubic unit cell and a lattice parameter of 1.0474 nm. Comparison between the powder diffraction data of $Eu_2Sn_2O_7$ (JCPDS, file No. 13-182) and those of $Y_2Sn_2O_7$ reveals that the strongest (222) peak is located at slightly different 2θ angles: 29.55° for

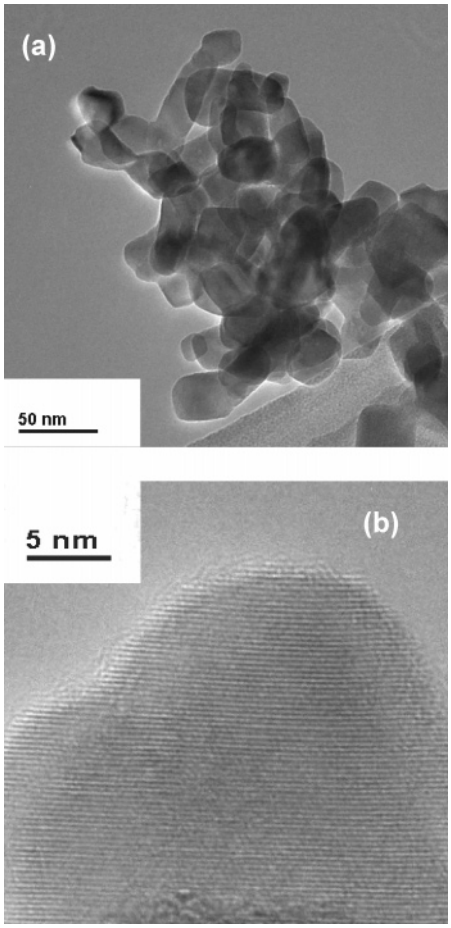

Figure 4. (a) TEM and (b) HRTEM images of the $Y_2Sn_2O_7$ film heat-treated at 1000 °C.

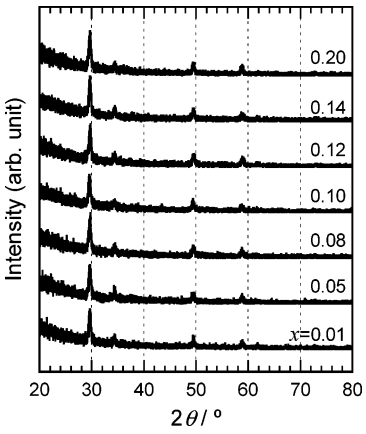

Figure 5. XRD patterns of $(Y_{1-x}Eu_x)_2Sn_2O_7$ ($x = 0.01-0.20$) films obtained by heating the dip-coated precursor solutions at 1000 °C for 1 h in air.

$Eu_2Sn_2O_7$ and 29.81° for $Y_2Sn_2O_7$. The 2θ values observed in the XRD patterns for $(Y_{1-x}Eu_x)_2Sn_2O_7$ films are in the range 29.70−29.75°. Furthermore, the fwhm values of the (222) peaks are within 0.45° for all films. From these results we judged that $Eu_2Sn_2O_7$ was not formed in our $(Y_{1-x}Eu_x)_2Sn_2O_7$ films. This will be supported by photoluminescence measurements for Eu^{3+} ions later.

The chemical state of yttrium, europium, tin, and oxygen in $(Y_{1-x}Eu_x)_2Sn_2O_7$ films was analyzed by XPS. Figure 6 shows XPS spectra for $(Y_{1-x}Eu_x)_2Sn_2O_7$ films ($x = 0$, 0.01, and 0.10) heat-treated at 1000 °C for 1 h in air in the Y 3d, Eu 4d, Sn 3d, and O 1s regions. The spectra of the Y 3d

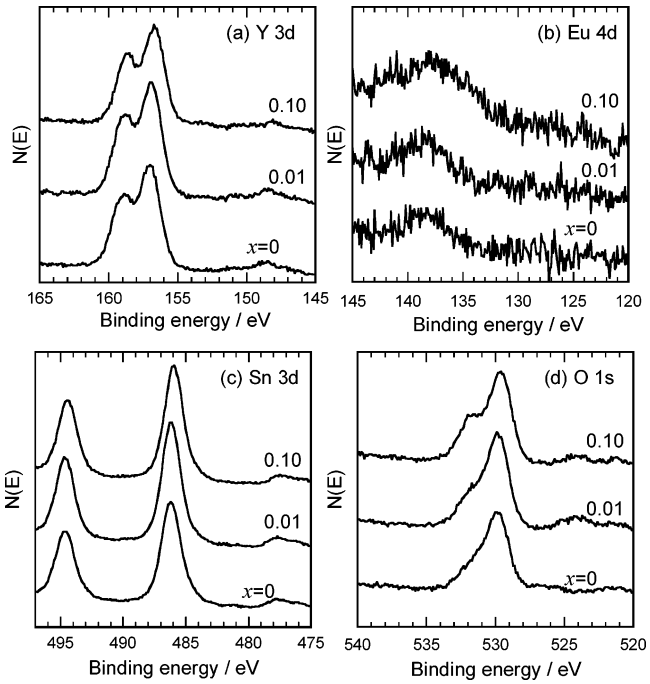

Figure 6. XPS spectra for $(Y_{1-x}Eu_x)_2Sn_2O_7$ films ($x = 0$, 0.01, and 0.10) heat-treated at 1000 °C for 1 h in air in the (a) Y 3d, (b) Eu 4d, (c) Sn 3d, and (d) O 1s regions.

core region (Figure 6a) exhibit spin−orbit splitting with two components of Y $3d_{3/2}$ (158.8 eV) and Y $3d_{5/2}$ (157.0 eV). The peak positions are close to those of Y_2O_3,[11] implying the presence of Y−O bonding in the films. In addition, the area ratio of Y $3d_{5/2}$ and $3d_{3/2}$ is close to 1.5, which is usually observed in Y_2O_3.[12] Another important aspect is that no Y−O−Si bonding exists in our films, judging from the fact that the Y $3d_{3/2}$ and $3d_{5/2}$ energy levels are much higher in yttrium silicate such as $Y_2Si_2O_7$ and Y_2SiO_5.[13] This indicates that the films did not react with the quartz glass substrate. In trivalent europium oxide (Eu_2O_3) the core-level spin−orbit splitting of Eu $4d_{3/2}$ and $4d_{5/2}$ lies between 135 and 142.5 eV.[14] Small and broad peaks can be seen in this energy region in spectra of the Eu 4d core level, as shown in Figure 6b. The relatively low Eu^{3+} doping levels ($x = 0.01$ and 0.10 in $(Y_{1-x}Eu_x)_2Sn_2O_7$) are responsible for the small Eu 4d peaks observed for our films. The broadness comes from multiplet splitting due to the strong exchange interaction between possible 4d core holes and the partly filled 4f shell.[14,15] The spin−orbit splitting of the Sn 3d level can be seen as two peaks appearing at 486.4 ($3d_{5/2}$) and 494.5 eV ($3d_{3/2}$), as shown in Figure 6c. This result clearly demonstrates the presence of Sn−O bonding in the films. Although distinguishing between Sn^{4+} and Sn^{2+} is difficult due to their similar binding energies in the XPS spectra of SnO_2 and SnO,[16] the nominal compositions of $(Y_{1-x}Eu_x)_2Sn_2O_7$ do not

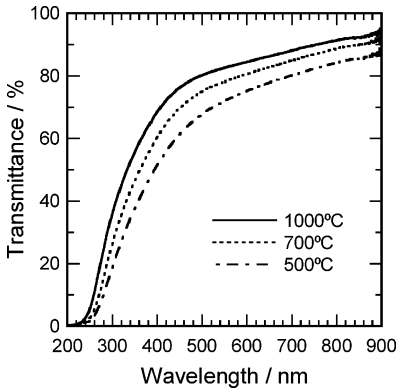

Figure 7. Optical transmission spectra of $(Y_{1-x}Eu_x)_2Sn_2O_7$ ($x = 0.10$) films heat-treated at 500, 700, and 1000 °C.

influence the initial valence state of tin (+4) at any doping level of x. The binding energy of the O 1s level observed at approximately 529.7 eV in Figure 6d is close to that of Y_2O_3 (529.5 eV).[13] The oxygen in SnO_2 also has a similar binding energy (530.5 eV).[17] Shoulders appearing at approximately 531.5 eV are ascribed to hydroxyl groups (OH−) that are likely acquired during exposure of the films to ambient water.[13,17] The XRD and XPS results indicate that our films can be identified as crystalline and pure $(Y_{1-x}Eu_x)_2Sn_2O_7$ phases.

3.3. Optical Properties of $(Y_{1-x}Eu_x)_2Sn_2O_7$ Films. Optical transmission of the $(Y_{1-x}Eu_x)_2Sn_2O_7$ films was slightly influenced by their structure and crystallinity, which depended on the heat-treatment temperature as indicated in Figure 2. Transmission spectra of the $(Y_{1-x}Eu_x)_2Sn_2O_7$ films ($x = 0.10$) that were heat-treated at 500, 700, and 1000 °C are shown in Figure 7. The film heated at a low temperature of 500 °C exhibits a gradual decrease of transmittance with decreasing wavelengths down to approximately 260 nm. The film seems to be in an amorphous state according to the XRD data and contains residual carbon species, which possibly absorb visible light, judging from the TG−DTA data. Actually, transmittance can be improved when the heating temperature is elevated to 600 (a spectrum is not shown) and 700 °C to burn out carbon species, although the films are still amorphous. Upon crystallization into the pyrochlore structure at heating temperatures of 800, 900, and 1000 °C, transmittance is more than 75% in the visible region, and hence, the films appeared highly transparent to the naked eye. It should be noted that the film itself has a higher transparency, taking account of the reflection loss at air/film/substrate interfaces on both sides of the substrate due to the dip-coating method employed in the present work.

The relationship between the film structure and optical properties was further examined by monitoring photoluminescence (PL) of the Eu^{3+} ions. Figure 8a shows PL spectra of $(Y_{1-x}Eu_x)_2Sn_2O_7$ films ($x = 0.10$) heat-treated at 500 and 700 °C. A spectral structure for the film heated at 500 °C is typical of Eu^{3+} present in the amorphous host. Similar PL spectra can be seen for Eu^{3+} doped in gels and glasses.[4,18−20]

(11) Moulder, J. F.; Stickle, W. F.; Sobol, P. E.; Bomben, K. D. *Handbook of X-ray Photoelectron Spectroscopy*; Perkin-Elmer Corp.: Eden Prairie, MN, 1992.
(12) Cho, M. H.; Ko, D. H.; Jeong, K.; Whangbo, S. W.; Whang, C. N.; Choi, S. C.; Cho, S. J. *Thin Solid Films* **1999**, *349*, 266.
(13) Chambers, J. J.; Parsons, G. N. *J. Appl. Phys.* **2001**, *90*, 918.
(14) Schneider, W. D.; Laubschat, C.; Nowik, I.; Kaindl, G. *Phys. Rev. B* **1981**, *24*, 5422.
(15) de Groot, F. *Coord. Chem. Rev.* **2005**, *249*, 31.
(16) Szuber, J.; Czempik, G.; Larciprete, R.; Koziej, D.; Adamowicz, B. *Thin Solid Films* **2001**, *391*, 198.
(17) Gaggiotti, G.; Galdikas, A.; Kačiulis, S.; Mattogno, G.; Šetkus, A. *J. Appl. Phys.* **1994**, *76*, 4467.
(18) Hayakawa, T.; Selvan, S. T.; Nogami, M. *J. Lumin.* **2000**, *87−89*, 532.

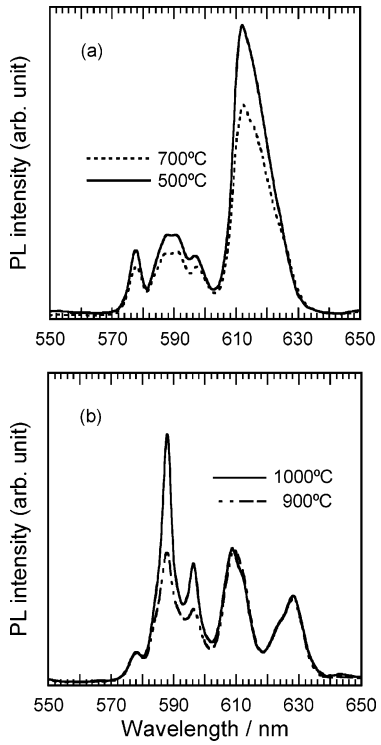

Figure 8. PL spectra of $(Y_{1-x}Eu_x)_2Sn_2O_7$ ($x = 0.10$) films heat-treated at (a) 500 and 700 °C and (b) 900 and 1000 °C. The excitation wavelength used was 254 nm.

A broader and stronger emission band with a peak at 612 nm is ascribed to the electric−dipole $^5D_0 \rightarrow {}^7F_2$ transition of the Eu^{3+} ions located inhomogeneously at the sites without inversion symmetry. A weaker emission band ranging from 580 to 600 nm is due to the magnetic−dipole $^5D_0 \rightarrow {}^7F_1$ transition. A minor emission peak for the $^5D_0 \rightarrow {}^7F_0$ transition is also observed at 577 nm. Thus, the asymmetry ratio, defined as $I[^5D_0 \rightarrow {}^7F_2]/I[^5D_0 \rightarrow {}^7F_1]$ (I emission intensity) is more than unity for the film heated at 500 °C. An increase in the heating temperature to 700 °C does not change the spectral structure, thereby indicating that Eu^{3+} ions are still present in the amorphous host. This observation coincides with the XRD and transmittance results as described above. In contrast, films heated at 900 and 1000 °C exhibit a different spectral structure as shown in Figure 8b. Enhanced, sharpened, and split $^5D_0 \rightarrow {}^7F_1$ emissions are observed at 588 and 596 nm, while $^5D_0 \rightarrow {}^7F_2$ emissions are reduced and split at 610 and 628 nm. As a result, the asymmetry ratio becomes less than unity.

Pyrochlore has a face-centered cubic structure (space group *Fd*3*m*) with eight formula units per conventional unit cell.[21] In the ideal $A_2B_2O_7$ pyrochlore structure the *A* site is a distorted cube and the *B* site is a regular octahedron.[6] The coordination is 8-fold for the *A* site and 6-fold for the *B* site. In $Y_2Sn_2O_7$, therefore, Y^{3+} and Sn^{4+} are surrounded by eight and six oxygen ions, respectively. Because eight oxygen ions form a distorted cube, the Y^{3+} site symmetry is lowered to D_{3d}.[22] The charge and ionic radii of Eu^{3+} (1.066 Å for the coordination number of 8)[23] would prefer substitution for Y^{3+} (1.019 Å) rather than for Sn^{4+} (0.69 Å) in the $Y_2Sn_2O_7$ lattice. Assuming that Eu^{3+} is located at the site with D_{3d} symmetry, the enhanced and sharpened $^5D_0 \rightarrow {}^7F_1$ emissions of Eu^{3+} in the $Y_2Sn_2O_7$ host crystal can be reasonably explained by the allowed magnetic−dipole transition due to the presence of an inversion center. Nevertheless, the split $^5D_0 \rightarrow {}^7F_2$ emissions coexist in the spectra even for the highly crystalline $(Y_{0.9}Eu_{0.1})_2Sn_2O_7$ film that was heated at 1000 °C.

The present situation is very different from the case of Eu^{3+} doped in cubic fluorite-type CeO_2 (space group *Fm*3*m*). When a small number of Eu^{3+} ions (typically 1 at. %) occupy the Ce^{4+} site with higher O_h symmetry, the electric−dipole $^5D_0 \rightarrow {}^7F_2$ transition is strictly forbidden.[24,25] Local distortion and/or oxygen vacancies possibly induced by the aliovalent dopant appear to have almost no influence on luminescence. This may result from the relatively low concentrations of the dopant. Under this condition oxygen vacancies are thought to be located around the Ce^{4+} ions, according to X-ray absorption fine structure spectroscopy (XAFS) studies.[26] On the other hand, lanthanide ions can exhibit electric−dipole transitions when they are doped in fluorite-type $Ce_yZr_{1-y}O_2$ solid solutions ($y = 0.60-0.20$) having lower D_{2d} site symmetry for metal ions (space group $P4_2/nmc$).[25]

It is then considered that the distorted $A^{3+}O_8$ cubic in the pyrochlore undergoes further modulation by introducing Eu^{3+}. That is, the $Eu^{3+}O_8$ cubic is locally more distorted than the $Y^{3+}O_8$ cubic for lattice relaxation. Judging from the PL spectra, both the $^5D_0 \rightarrow {}^7F_1$ and the $^5D_0 \rightarrow {}^7F_2$ emissions from $(Y_{0.9}Eu_{0.1})_2Sn_2O_7$ are dominated by inhomogeneous broadening that reflects the site-to-site variation in the local structure around Eu^{3+}. Such variation is more obviously implicated in the $^5D_0 \rightarrow {}^7F_0$ transition, where the corresponding energy levels are nondegenerate. Broadening of the $^5D_0 \rightarrow {}^7F_0$ transition in the PL spectra directly proves the presence of Eu^{3+} luminescent centers having various local environments.[27] In summary of the PL properties, luminescence of $(Y_{1-x}Eu_x)_2Sn_2O_7$ is characterized as multiband orange-red emissions with five intense peaks at around 577, 588, 596, 610, and 628 nm. The chromaticity then corresponds to a region between pink and yellowish pink in the CIE diagram.

Figure 9 shows PL excitation spectra for the 588 and 610 nm emissions of $(Y_{1-x}Eu_x)_2Sn_2O_7$ film ($x = 0.10$) heat-treated at 1000 °C. Both emissions originate from a similar broadband excitation centered at 263 nm. This fact may exclude the possibility that there exists two different sites

(19) Sun, B.; Song, H.; Wang, J.; Peng, H.; Zhang, X.; Lu, S.; Zhang, J.; Xia, H. *Chem. Phys. Lett.* **2003**, *368*, 412.
(20) Hreniak, D.; Jasiorski, M.; Maruszewski, K.; Kepinski, L.; Krajczyk, L.; Misiewicz, J.; Strek, W. *J. Non-Cryst. Solids* **2002**, *298*, 146.
(21) Jana, Y. M.; Sengupta, A.; Ghosh, D. *J. Magn. Magn. Mater.* **2002**, *248*, 7.
(22) López-Navarrete, E.; Orera, V. M.; Lázaro, F. J.; Carda, J. B.; Ocana, M. *J. Am. Ceram. Soc.* **2004**, *87*, 2108.
(23) Shanon, R. D. *Acta Crystallogr., A* **1976**, *32*, 751.
(24) Fujihara, S.; Oikawa, M. *J. Appl. Phys.* **2004**, *95*, 8002.
(25) Fornasiero, P.; Speghini, A.; Di Monte, R.; Bettinelli, M. Kašpar, J.; Bigotto, A.; Sergo, V.; Graziani, M. *Chem. Mater.* **2004**, *16*, 1938.
(26) Yamazaki, S.; Matsui, T.; Ohashi, T.; Arita, Y. *Solid State Ionics* **2000**, *136*−*137*, 913.
(27) Bazzi, R.; Flores, M. A.; Louis, C.; Lebbou, K.; Zhang, W.; Dujardin, C.; Roux, S.; Mercier, B.; Ledoux, G.; Bernstein, E.; Perriat, P.; Tillement, O. *J. Colloid Interface Sci.* **2004**, *273*, 191.

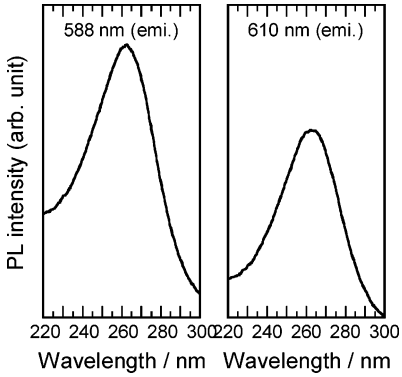

Figure 9. PL excitation spectra of $(Y_{1-x}Eu_x)_2Sn_2O_7$ ($x = 0.10$) film heat-treated at 1000 °C. The emission wavelengths used were 588 and 610 nm.

in terms of symmetry for Eu^{3+} in $(Y_{1-x}Eu_x)_2Sn_2O_7$, which was invoked by the simultaneous occurrence of the electric−and magnetic−dipole transitions. It should be noted that bixbyite-type cubic Y_2O_3 (space group *Ia3*) has two kinds of Y^{3+} sites. Therefore, Eu^{3+} ions in the well-known Y_2O_3:Eu^{3+} red phosphor occupy the site with S_6 or C_2 symmetry. Because the S_6 site has an inversion center, Eu^{3+} in this site shows only the magnetic−dipole transition. It has been reported that the energy of the charge-transfer state of Eu^{3+} at the S_6 site is higher than that at the C_2 site, probably due to shorter Y−O bonds for the former.[28] This was demonstrated by the excitation band occurring at higher energy for the $^5D_0 \rightarrow {}^7F_1$ emission (Eu^{3+} at the S_6 site) than for the $^5D_0 \rightarrow {}^7F_2$ emission (Eu^{3+} at the C_2 site). Because this energy shift is not observed for $(Y_{1-x}Eu_x)_2Sn_2O_7$, the site symmetry depending on site-to-site variation is not distinguishable. A comparison between the transmittance spectra (Figure 7) and the PL excitation spectra (Figure 9) indicates that the Eu^{3+} is excited largely through charge transfer from O^{2-}. Many Eu^{3+}-doped oxide materials including pyrochlores have the charge-transfer ($O^{2-} - Eu^{3+}$) band in a similar wavelength region.[29−32] If the host lattice excitation was dominant, shorter wavelength tails of the excitation spectra should have higher intensities.

The dependence of the PL properties on the Eu^{3+} doping levels in $(Y_{1-x}Eu_x)_2Sn_2O_7$ was examined. Figure 10a compares PL spectral structure of the $(Y_{1-x}Eu_x)_2Sn_2O_7$ films ($x = 0.01$, 0.10, and 0.20). At $x = 0.01$, emissions can be seen due to the $^5D_0 \rightarrow {}^7F_0$, $^5D_0 \rightarrow {}^7F_1$, and $^5D_0 \rightarrow {}^7F_2$ transitions of Eu^{3+}, although their intensities are relatively weak because of the low doping level. The PL intensities show an approximately 7-fold increase for the film of $x = 0.10$ without changing the spectral structure. The intensities are then reduced for the film of $x = 0.20$, indicating the occurrence of concentration quenching due to the multipole−multipole and/or the superexchange interaction between the Eu^{3+} ions. Figure 10b shows the effect of the Eu^{3+} doping levels on the PL intensity, $I[^5D_0 \rightarrow {}^7F_1]$. The intensity increases upon increasing the doping level up to $x = 0.10$

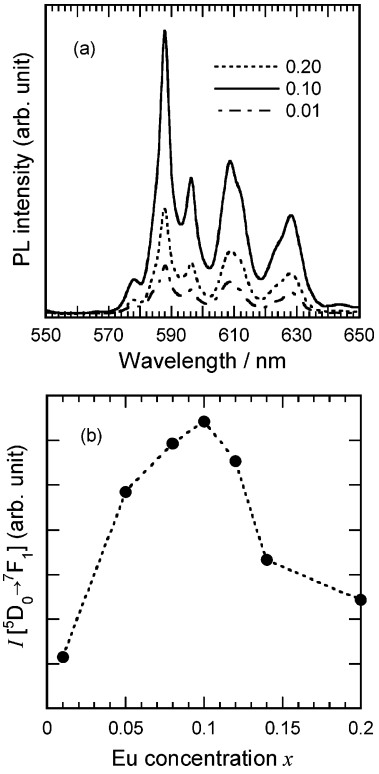

Figure 10. (a) PL spectra of $(Y_{1-x}Eu_x)_2Sn_2O_7$ ($x = 0.01$, 0.10, and 0.20) films heat-treated at 1000 °C. The excitation wavelength used was 254 nm. (b) Relationship between the Eu^{3+} concentration (x in $(Y_{1-x}Eu_x)_2Sn_2O_7$) and PL intensity, $I[^5D_0 \rightarrow {}^7F_1]$.

and then decreases, thereby providing the critical concentration of 10 at. % of Y^{3+} in the $Y_2Sn_2O_7$ host. This value is comparable to that reported for the Y_2O_3:Eu^{3+} phosphor.[33,34] It can then be concluded that the Eu^{3+} ions are homogeneously distributed in the $Y_2Sn_2O_7$ lattice in the present thin-film samples.

Generally, it is not easy to observe a local distortion in the crystal lattice arising from elemental substitution, as in the case of Eu^{3+} for Y^{3+} in $(Y_{1-x}Eu_x)_2Sn_2O_7$. Efforts have been made, however, to analyze such a distortion in the red phosphors of YBO_3:Eu^{3+} and Y_2O_3:Eu^{3+} using XAFS.[35,36] It was shown that the levels of disorder around the Eu^{3+} ions were dependent not on the Eu^{3+} concentration, but on the crystallinity. This experimental fact indicates that the luminescent properties of Eu^{3+} are determined by the crystallinity and the lattice symmetry of the host crystal rather than the local distortion induced by substitution. As mentioned above, the spectral structure for Eu^{3+} luminescence is unchanged among the three doping levels of $x = 0.01$, 0.10, and 0.20 in $(Y_{1-x}Eu_x)_2Sn_2O_7$. If the change of the local structure influenced the luminescent properties of Eu^{3+}, the spectral structure would also be changed. Therefore, it can be said that the multiband emissions are an intrinsic physical property of the $(Y_{1-x}Eu_x)_2Sn_2O_7$ films.

(28) Jia, M.; Zhang, J.; Lu, S.; Sun, J.; Luo, Y.; Ren, X.; Song, H.; Wang, X. J. *Chem. Phys. Lett.* **2004**, *384*, 193.
(29) Dorenbos, P. *J. Lumin.* **2005**, *111*, 89.
(30) McCauley, R. A.; Hummel, F. A. *J. Lumin.* **1973**, *6*, 105.
(31) Brixner, L. H. *Mater. Res. Bull.* **1984**, *19*, 143.
(32) Lu, Z.; Wang, J.; Tang, Y.; Li, Y. *J. Solid State Chem.* **2004**, *177*, 3075.
(33) Pang, M. L.; Lin, J.; Cheng, Z. Y.; Fu, J.; Xing, R. B.; Wang, S. B. *Mater. Sci. Eng. B* **2003**, *100*, 124.
(34) Chong, M. K.; Pita, K.; Kam, C. H. *J. Phys. Chem. Solids* **2005**, *66*, 213.
(35) Wei, Z. G.; Sun, L. D.; Jiang, X. C.; Liao, C. S.; Yan, C. H. *Chem. Mater.* **2003**, *15*, 3011.
(36) Qi, Z.; Shi, C.; Zhang, W.; Zhang, W.; Hu, T. *Appl. Phys. Lett.* **2002**, *81*, 2857.

4. Conclusions

In summary, we fabricated and investigated the photoluminescent properties of the pyrochlore-structured $(Y_{1-x}Eu_x)_2Sn_2O_7$ films. XRD, HRTEM, and XPS examinations revealed that the films were highly crystalline without precipitation of any other phases and suitable for optical measurements. PL spectra indicated the occurrence of the multiband orange-red luminescence at a single-wavelength excitation due to the weak $^5D_0 \rightarrow {}^7F_0$ transition and the doubly split $^5D_0 \rightarrow {}^7F_1$ and $^5D_0 \rightarrow {}^7F_2$ transitions. Inhomogeneous broadening arising from the site-to-site variation of Eu^{3+} could also be observed. These spectral features provided the chromaticity of a region between pink and yellowish pink in the CIE diagram, which would be adequate to use as a new reddish component in reproducing natural light in optical devices.

CM0513785